


RESEARCH ARTICLE

Relaxometry and quantification in sodium MRI of cerebral gliomas: A FET-PET and MRI small-scale study

Wieland A. Worthoff¹  | Aliaksandra Shymanskaya²  | Johannes Lindemeyer¹ |
Karl-Josef Langen^{1,3}  | N. Jon Shah^{1,2,4} 

¹Institute of Neuroscience and Medicine - 4,
Forschungszentrum Jülich, Jülich, Germany

²Institute of Neuroscience and Medicine - 11,
Forschungszentrum Jülich, Jülich, Germany

³Department of Nuclear Medicine, RWTH
Aachen University, JARA, Aachen, Germany

⁴Department of Neurology, RWTH Aachen
University, JARA, Aachen, Germany

Correspondence

Wieland A. Worthoff, Institute of
Neuroscience and Medicine –
4, Forschungszentrum Jülich GmbH, 52425,
Jülich, Germany.
Email: w.worthoff@fz-juelich.de

Sodium MRI is a promising method for assessing the metabolic properties of brain tumours. In a recent study, a strong relationship between semi-quantitative abnormalities in sodium MRI and the mutational status of the isocitrate dehydrogenase enzyme (IDH) with untreated cerebral gliomas was observed. Here, sodium relaxometry in brain tumour tissue was investigated in relation to molecular markers in order to reveal quantitative sodium tissue parameters and the differences between healthy tissue and brain tumour. The previous semi-quantitative approach is extended by use of suitable relaxometry methods accompanied by numerical simulation to achieve detailed quantitative analysis of intra- and extracellular sodium concentration using an enhanced SISTINA sequence at 4 T. Using optimised techniques, biexponential sodium relaxation times in tumour (T_{2f}^* , T_{2s}^*) and in healthy contralateral brain tissue ($T_{2f,CL}^*$, $T_{2s,CL}^*$) were estimated in 10 patients, along with intracellular sodium molar fractions (χ , χ_{CL}), volume fractions (η , η_{CL}) and concentrations (ρ_{in} , $\rho_{in,CL}$). The total sodium tissue concentrations (ρ_T , $\rho_{T,CL}$) were also estimated. The ratios $T_{2f}^*/T_{2f,CL}^*$ ($P = .05$), η/η_{CL} ($P = .02$) and χ/χ_{CL} ($P = .02$) were significantly lower in IDH mutated than in IDH wildtype gliomas ($n = 4$ and $n = 5$ patients, respectively). The Wilcoxon rank-sum test was used to compare sodium MRI parameters in patients with and without IDH mutation. Thus, quantitative analysis of relaxation rates, intra- and extracellular sodium concentrations, intracellular molar and volume fractions based on enhanced SISTINA confirmed a relationship between abnormalities in sodium parameters and the IDH mutational status in cerebral gliomas, hence catering for the potential to provide further insights into the status of the disease.

KEYWORDS

enhanced SISTINA, gliomas, IDH mutational status, relaxometry, sodium metabolic imaging

Abbreviations used: CL, contralateral; FET, O-(2-[¹⁸F]fluoroethyl)-L-tyrosine; FOV, field of view; GM, grey matter; IDH, isocitrate dehydrogenase enzyme; ISMF, intracellular sodium molar fraction; ISVF, intracellular sodium volume fraction; MQC, multiple quantum coherence; NAWM, normal-appearing white matter; RF, radio frequency; SISTINA, simultaneous single-quantum and triple-quantum-filtered MRI of ²³Na; SNR, signal-to-noise ratio; SQ, single quantum; SQC, single quantum coherence; TQ, triple quantum; TQC, triple quantum coherence; UTE, ultrashort echo time; WHO, World Health Organization; WM, white matter.

Wieland A. Worthoff and Aliaksandra Shymanskaya both contributed equally to this study

This is an open access article under the terms of the Creative Commons Attribution-NonCommercial-NoDerivs License, which permits use and distribution in any medium, provided the original work is properly cited, the use is non-commercial and no modifications or adaptations are made.

© 2020 The Authors. NMR in Biomedicine published by John Wiley & Sons Ltd

1 | INTRODUCTION

Cerebral gliomas are primary brain tumours¹ and are classified into different grades according to the World Health Organization (WHO) definition. In this classification, the molecular genetic profile, for example, the gene mutation encoding for the isocitrate dehydrogenase enzyme (IDH) plays an important role² and it is accepted that patients with IDH wildtype gliomas have a worse prognosis than patients with IDH mutated gliomas. Currently, the determination of the IDH mutational status requires a brain biopsy and consequently there is great interest in imaging methods to determine this parameter noninvasively.³ MR spectroscopic methods have been suggested,^{4–6} but typically suffer from a long measurement time or low spatial coverage.

Sodium plays an essential role in human cell physiology and can be measured noninvasively *in vivo* via MRI due to its noninteger nuclear spin.^{7,8} In a so-called “two-compartment” model of brain tissue,⁹ sodium is present in two environments, that is, in restricted and nonrestricted spaces, which are also largely associated with intra- and extracellular spaces,¹⁰ and the mean sodium distribution is described by the tissue sodium concentration. The compartments can be detected separately due to the difference in sodium concentration and spin dynamics,¹¹ which are dependent on the chemical environment of sodium ions inside and outside cells, and are controlled by the sodium-potassium pump.⁷ Deviations from normal cell metabolism can lead to dysfunction of the sodium-potassium pump and a redistribution of sodium between the compartments, a change in cell volume, and the malfunction of cells due to separate ion regulatory mechanisms.^{12–14} While some studies exist that dispute that theory in blood and heart tissue,^{15–17} studies in human brain used this model consistently.^{11,18–23} In the following text it is assumed that the intracellular compartment is dominated by restricted sodium, while the extracellular compartment is dominated by nonrestricted sodium.

The chemical environment determines the spin dynamics of sodium nuclei, mainly through the interaction between electric field gradients modulated by molecular motion and the sodium quadrupolar moment. In a restricted environment, sodium relaxes biexponentially with two relaxation constants: a fast component, T_{2f} , and a slow component, T_{2s} . Furthermore, triple quantum coherences (TQCs) can evolve from single quantum coherences (SQCs) under certain conditions.^{19,20,22} In the nonrestricted space, sodium possesses a single relaxation time, T_{ex} .

In a recent study, a strong relationship was observed between semi-quantitative measures of abnormalities in sodium MRI and the IDH mutational status in 10 patients with untreated cerebral gliomas. Sodium MRI was found to be superior to PET using [¹⁸F]-fluoroethyltyrosine for identifying the IDH mutational status.²⁴ The reasons for the different sodium distribution in IDH mutant and IDH wild-type tumours are not yet fully understood. It has been shown that IDH mutant and IDH wildtype tumour cells exhibit significant differences in their metabolic profile.²⁵ Current hypotheses for the different sodium distributions in tumours are an enlargement of the interstitial fluid compartment caused by the leakage of plasma proteins, an exhaustion of the ATP level in rapidly proliferating cells, which is necessary to maintain the sodium gradient, or dysfunction of cellular sodium channels.²⁶

Enhanced SISTINA is a modified triple quantum filter with two separate readouts: an ultrashort echo time (UTE) readout train after the first hard RF pulse, and a Cartesian, multiple gradient echo readout after the third hard RF pulse, which yields information about single-quantum (SQ) and triple-quantum (TQ) coherences after the application of an appropriate phase cycle scheme.²⁷ In previous studies,^{23,28} the sequence obtained sodium tissue relaxation times T_{2f}^* and T_{2s}^* in healthy tissue and allowed the estimation of sodium tissue parameters from sodium images²⁹ for the supposed tissue model. It was assumed that SQCs originated from both restricted (mostly intracellular sodium) and nonrestricted sodium (mostly extracellular sodium), while TQCs evolved largely in a restricted environment only.^{19,20,22,23} In the current study, this approach was extended to a detailed quantitative analysis of sodium concentration in restricted and unrestricted environments in the aforementioned group of brain tumour patients, in order to shed light into the basic mechanisms of this promising approach of predicting IDH mutation status noninvasively. In order to obtain further insights into the dynamics of the relaxation processes, a quantification of the two-compartment tissue model was created. This model relies on several sodium parameters, such as intra- and extracellular sodium concentrations, intracellular molar and volume fractions, total sodium concentration, and the relaxation times of sodium. Numerical ROIs with several realistic combinations of these parameters (provided below in the Methods section) and using signal relaxation behaviour derived from quantum mechanical description of density matrix evolution were created. The time dependence was investigated on the timescale upon which the patient measurements were performed. This numerical modelling of sodium in tissue is used to optimise the curve-fitting procedure and thus assists in the quantification process. However, the parameter estimation in this study has been based on the assumption of an adequate two-compartment model, nevertheless, verification of this model has not been performed.

2 | THEORY

As observed in Shymanskaya et al.,²⁴ the ratio of total sodium to restricted sodium in tissue is dependent on the mutational status of the tumour; the increase of total sodium and the change in the restricted sodium fraction can be reflected in the change of the intracellular sodium molar fraction (ISMF) χ , which is defined as the fraction of the molar content sodium M_{in} inside the cells divided by the total sodium molar content $M_T = M_{ex} + M_{in}$, $\chi = M_{in}/M_T$. If the amount of nonrestricted sodium is significantly increased in tissue, and χ is low, the relaxation behaviour of the sodium signal might be dominated by the relaxation time of the nonrestricted sodium T_{ex} .

3 | METHODS: RELAXOMETRY AND SIMULATIONS

3.1 | Relaxometry using enhanced SISTINA

The enhanced SISTINA sequence and the relaxometry routine used for the estimation of relaxation times have been described elsewhere.^{23,28} Here, however, the application of these methods is studied for different tissue compositions. The UTE data are weighted by total sodium, which consist of restricted sodium (relaxing with fast relaxation time T_{2f}^* and slow relaxation time T_{2s}^*) and nonrestricted sodium (relaxing with T_{ex}^*). The TQ images are weighted by the presence of restricted sodium, which relaxed biexponentially with T_{2f}^* and T_{2s}^* .

3.2 | Numerical tissue model

In order to investigate the applicability of the methods from the earlier studies^{23,28} to the diseased tissue, several simulations were performed. For these simulations, numerical datasets with different sodium tissue parameters were created to serve as numerical phantoms. The sodium tissue parameters included intra- and extracellular sodium concentrations, intracellular volume and molar fractions, and relaxation times. The relaxometry-fitting routines were performed, where the same echo times were selected as in patient measurements, with noise added using the Monte Carlo method. The whole procedure is summarised in Figure 1. In the first step, the accuracy of the T_{2f}^* estimation was evaluated. These results were used to choose a better-suited fit routine for a certain tissue composition. Furthermore, these fit results were used to determine the accuracy of the T_{2s}^* estimation.

3.3 | UTE relaxometry

The first set of simulations was performed on the UTE data to estimate the influence of tissue parameters on the estimation of T_{2f}^* . For this purpose, multi-exponential gradient echo data were generated using Equation 1A, with fast and slow relaxation times T_{2f}^* and T_{2s}^* , the magnetisation amplitude of the restricted sodium M_{in} , extracellular relaxation time T_{ex} , and ISMF χ . In this case, the amount of nonrestricted sodium is $M_{ex} = M_{in}(1-\chi)\chi^{-1}$.

$$S_{UTE} = M_{in} \left[3 \exp\left(-\frac{TE_{UTE}}{T_{2f}^*}\right) + 2 \exp\left(-\frac{TE_{UTE}}{T_{2s}^*}\right) \right] + M_{in} \frac{1-\chi}{\chi} \exp\left(-\frac{TE_{UTE}}{T_{ex}^*}\right) \quad (1A)$$

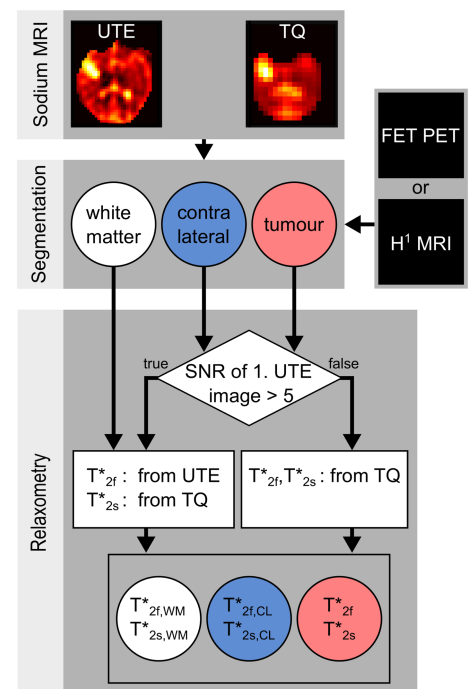


FIGURE 1 Fast and slow relaxation rates for tumour, contralateral tissue and white matter are obtained from the dynamics of UTE and TQ filtered datasets through the appropriate choice of fitting routine

Rician noise was added to the magnitude images using MATLAB, as described in Gudbjartsson and Patz.³⁰ Simulations were performed using 10 000 instances of noise generated with the Monte Carlo method. In the region of no signal, the noise obeys a Rayleigh distribution.³⁰ The unbiased signal Σ was estimated by correcting the signal amplitude to reduce the effect of noise by using $\Sigma = \sqrt{|\text{mean}(\text{signal})^2 - \sigma_{\text{noise}}^2|}$, with the standard deviation of the noise distribution σ_{noise} , and $\text{SNR} = \Sigma \cdot \sigma_{\text{noise}}^{-1}$.

3.4 | UTE relaxometry: T_{2f}^* estimation method 1

This simulation was performed for the case investigated in Worthoff et al.²³ Standard deviation of noise σ_{noise} and M_{in} were chosen according to the required SNR value, comparable with the values measured in white matter (WM) in the UTE images. The fitting function is given by Equation 1B, with the echo times TE_{UTE} , and offset G , representing the slow relaxation term.³¹

$$S_{\text{UTE}} = A \exp\left(-\frac{\text{TE}_{\text{UTE}}}{T_{2f,\text{fit}}^*}\right) + G \quad (1B)$$

Fits were performed for $T_{2f}^* = 1$ and 3 ms; $T_{2s}^* = 15, 20, 25$ and 30 ms; $T_{\text{ex}}^* = 55$ ms (for cases of $T_{\text{ex}}^* = 35, 45$ and 65 ms, no significant difference was observed); and $\chi = 0.1, 0.6$ and 0.8. M_{in} was chosen as a fixed value, so that in the case observed in normal tissue in Worthoff et al.,²³ $\text{SNR} = 4$ ($T_{2f}^* = 3$ ms, $T_{2s}^* = 30$ ms, $\chi = 0.6$), and in the case of low ISMF, $\text{SNR} = 11$ ($\chi = 0.1$). The corresponding errors were estimated, as suggested in Bouhrara et al.³²; the relative bias was calculated as $\Theta = 100 \cdot (T_{2f}^* - \text{mean}(T_{2f,\text{fit}}^*)) / T_{2f}^*$.

Furthermore, the dependence of the fitting performance of Equation 1B on the SNR of the first echo was estimated. In this simulation, χ was chosen to be 0.1 and 0.6. The fast relaxation times were $T_{2f}^* = 1$ ms and $T_{2f}^* = 3$ ms.

3.5 | UTE relaxometry: T_{2f}^* estimation method 2

The failure of the T_{2f}^* estimation method 1 (Equation 1B) for the low values of χ (see Results) suggested that in tissue with a negligible amount of fast-relaxing sodium, the fast relaxation constant could not be estimated reliably. Therefore, an alternative to the fitting routine used in the earlier studies^{23,28} was examined. In this case, the values were fitted to the function given in Equation 1C, where the value of $T_{\text{ex,fix}}^* = 55$ ms was fixed and the parameters K , $T_{2f,\text{fit}}^*$, and L were obtained.

$$S_{\text{UTE}} = K \exp\left(-\frac{\text{TE}_{\text{UTE}}}{T_{2f,\text{fit}}^*}\right) + L \exp\left(-\frac{\text{TE}_{\text{UTE}}}{T_{\text{ex,fix}}^*}\right) \quad (1C)$$

The simulations were performed for $T_{\text{ex,fix}}^*$ of 35, 45, 55 and 65 ms using Equation 1C, where 55 ms is the ground-truth value in Equation 1A.

The dependence of the fitting performance on the SNR values was also investigated for method 2. In these simulations, χ was 0.6 and 0.1, while the fast relaxation times were $T_{2f}^* = 1$ ms and $T_{2f}^* = 3$ ms. $T_{\text{ex,fix}}^* = 65$ ms was chosen to result in the maximum error in $T_{2f,\text{fit}}^*$.

3.6 | TQ relaxometry: T_{2s}^* estimation

Furthermore, the performance of the fitting routine, introduced in Worthoff et al.,²³ for the estimation of the slow relaxation time, T_{2s}^* , was evaluated. Multi-exponential gradient echo data were generated using Equation 2A, with the fast relaxation times $T_{2f,\text{fix}}^*$ taken from the results of the T_{2f}^* estimation methods 1 and 2 (see the supporting information Tables A1 and A3). T_{2s}^* was assumed to be 15, 20, 25 and 30 ms, and $\chi = 0.1, 0.6$ and 0.8. Only one compartment was considered to contribute to the signal. The fitting function is given in Equation 2B. Again, Rician noise was added. Simulations were performed using 10 000 instances of noise generated with the Monte Carlo method.

$$S_{\text{TQ}} = M_{\text{in}} \left[\exp\left(-\frac{\text{TE}_{\text{TQ}}}{T_{2f}^*}\right) - \exp\left(-\frac{\text{TE}_{\text{TQ}}}{T_{2s}^*}\right) \right] \left[\exp\left(-\frac{\tau}{T_{2f}^*}\right) - \exp\left(-\frac{\tau}{T_{2s}^*}\right) \right] \exp\left(-\frac{\delta}{T_{2s}^*}\right) \quad (2A)$$

$$S_{\text{TQ}} = D \left[\exp\left(-\frac{\text{TE}_{\text{TQ}}}{T_{2f,\text{fix}}^*}\right) - \exp\left(-\frac{\text{TE}_{\text{TQ}}}{T_{2s,\text{fit}}^*}\right) \right] \left[\exp\left(-\frac{\tau}{T_{2f,\text{fix}}^*}\right) - \exp\left(-\frac{\tau}{T_{2s,\text{fit}}^*}\right) \right] \exp\left(-\frac{\delta}{T_{2s,\text{fit}}^*}\right) \quad (2B)$$

The fitting performance was evaluated for the values acquired with T_{2f}^* estimation method 1 (Table A1) and method 2 (Table A3). The magnitude of M_{in} was chosen in such a way that for the case observed in Worthoff et al.,²³ SNR = 6 for $\chi = 0.6$ and $\chi = 0.8$, and SNR = 3.3 for $\chi = 0.1$. This allowed direct comparison of the sensitivity of the fitting routine from Equation 2B with the values of $T_{2f,fit}^*$ acquired from the fitting using Equation 1B and Equation 1C. However, caution is advised, because M_{in} was not proportional to ISMF (χ), and instead, it additionally depends on the change in M_{ex} and on relaxation times. Therefore, the value M_{in} assumed for the fits was calculated based not on the value of χ , but on the resulting value of the SNR.

Furthermore, as for the UTE echo fits, the dependence of the fitting performance of Equation 2B on the SNR of the first echo after the third RF pulse was estimated.

3.7 | TQ relaxometry: combined T_{2f}^* and T_{2s}^* estimation

As demonstrated in the Results section, the estimation of T_{2f}^* with the UTE fitting routines might be incorrect if a large portion of slow-relaxing sodium is present (low ISMF χ). Therefore, the possibility of estimating T_{2f}^* and T_{2s}^* from the TQ signal decay was considered under the assumption that only the restricted compartment generated TQ signal. The fit function is given by Equation 2C.

$$S_{TQ} = D \left[\exp\left(-\frac{TE_{TQ}}{T_{2f,fit}^*}\right) - \exp\left(-\frac{TE_{TQ}}{T_{2s,fit}^*}\right) \right] \left[\exp\left(-\frac{\tau}{T_{2f,fit}^*}\right) - \exp\left(-\frac{\tau}{T_{2s,fit}^*}\right) \right] \exp\left(-\frac{\delta}{T_{2s,fit}^*}\right) \quad (2C)$$

The performance of the fitting function from Equation 2C was simulated for T_{2f}^* and T_{2s}^* . T_{2f}^* was 1 and 3 ms, while T_{2s}^* was 15, 20, 25 and 30 ms. The dependence on the SNR was investigated. This routine was independent of T_{ex}^* .

4 | METHODS: QUANTITATIVE PATIENT MEASUREMENTS

4.1 | Patient cohort

Ten patients (four females aged 43 ± 12 years, and six males aged 54 ± 15 years) were referred from the Department of Nuclear Medicine of the University Clinic of Aachen, and underwent brain tumour assessment with [^{18}F]-FET-PET. Additionally, the patients were offered morphological proton imaging in a 4 T MRI scanner, as well as sodium imaging. All subjects gave prior informed written consent. The local ethics committee of the University of Aachen waived the requirement for additional approval due to the retrospective nature of the study. The study adheres to the standards established in the declaration of Helsinki.

The patients received a neuropathological diagnosis based on the 2016 WHO classification.² Grounded on biopsy, five patients were identified as having an untreated IDH mutated glioma (one astrocytoma WHO Grade II, three anaplastic astrocytoma WHO grade III, and one glioblastoma WHO grade IV), with an additional five patients having an untreated IDH wildtype glioma (three anaplastic glioma WHO Grade III, one diffuse midline glioma WHO IV, and one glioblastoma WHO grade IV). These are the same patients who were considered in Shymanskaya et al.²⁴ Further details regarding the patient cohort are provided in the supporting information, Table A10.

4.2 | [^{18}F]-FET-PET and tissue segmentation

The [^{18}F]-FET-PET measurements that were performed are described in Shymanskaya et al.²⁴ in more detail. [^{18}F]-FET-PET images were coregistered with proton MRI using MPI Tool (version 3.28, ATV, Kerpen, Germany). Tumour ROIs were chosen based either on the [^{18}F]-FET-PET scans, or on the proton MRI abnormalities. For the lesions without an abnormal [^{18}F]-FET uptake, an ROI was selected manually on the area of signal abnormality in T_1 - and T_2 -weighted transversal MR scans. In the tumours with increased [^{18}F]-FET uptake, the ROI was chosen as a circular ROI with a diameter of 1.6 cm in the transaxial slice around the lesion maximum. Contralateral (CL), normal-appearing brain including WM and grey matter (GM) was chosen as a reference ROI.³³ Furthermore, a region of healthy WM was manually segmented and used as a reference in case CL tissue was affected (Figure 2).

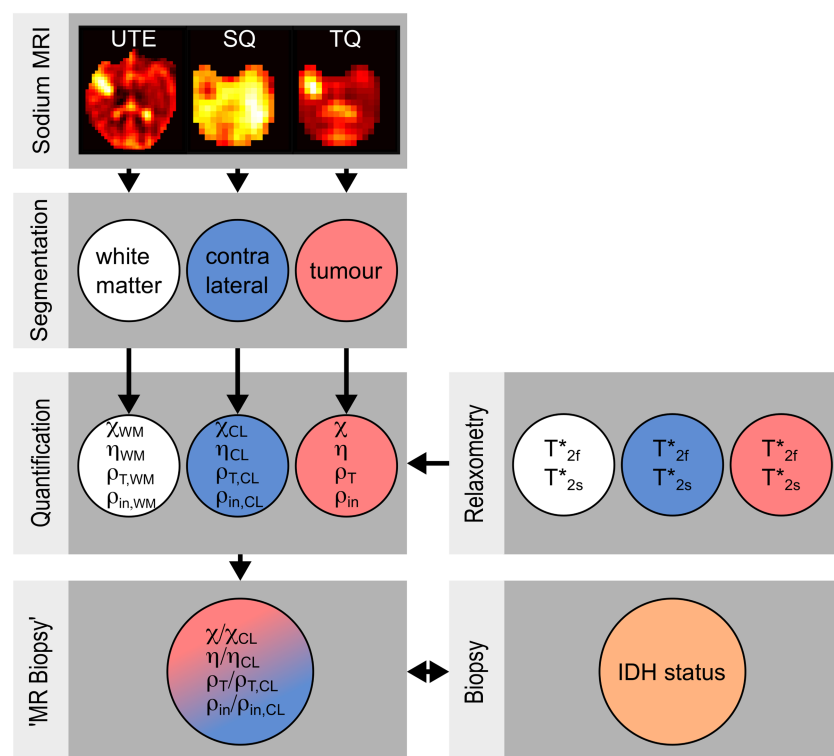


FIGURE 2 Quantitative tissue parameters are gathered from enhanced SISTINA datasets. Parameter ratios are compared with the IDH status found by biopsy

4.3 | Sodium measurements

Sodium imaging with the enhanced SISTINA sequence²³ was performed on a home-assembled 4 T MRI scanner centred around a Siemens (Siemens Healthineers AG, Germany) console and a Siemens Sonata whole-body gradient system capable of a maximum gradient strength of 40 mT/m and peak slew rate of 200 mT/m/s. The RF probe was a dual-tuned Na/H birdcage coil (Rapid Biomed GmbH, Germany). Sequence parameters are given in Table 1, with sequence timing and echo spacing being the same as in Worthoff et al.²³ Figure 3 shows exemplary enhanced SISTINA image data of two patients. The sodium images were coregistered with the proton MR images, and the UTE and Cartesian sodium images were coregistered among each other using the FSL library (FMRIB, Oxford, UK).^{34–36}

B_0 and B_1 corrections on the sodium images were performed during postprocessing. B_0 maps were acquired with a multiple-echo gradient echo sequence.

Flip angle maps with the field of view (FOV) and resolution matching those of the enhanced SISTINA sequence were acquired using the Bloch-Siegert method.³⁷ This involves the generation of two Cartesian images using a 2 kHz off-resonant Fermi pulse (flip angle 410° , pulse duration 5 ms).³⁸

TABLE 1 Parameters used for the acquisitions of the enhanced SISTINA images in 9 hours 52 minutes (TR = 150 ms)

Acquisition	TE [ms]	Bandwidth [Hz/pixel]	Imaging parameters
UTE	0.36, 1.75, 3.14, 4.53, 5.92	1,000	FOV: 320 x 240 x 160 mm ³ 3948 projections 44 points per half-out projection FWHM of PSF: 6 mm Regridded to 2.5 mm iso DISCOBALL sampling scheme ⁴⁶
SQ/TQ	7.0, 16.2, 25.3, 34.5, 43.6, 52.8	120	FOV: 320 x 240 x 160 mm ³ Voxel size: 10 mm iso Cartesian MGRE

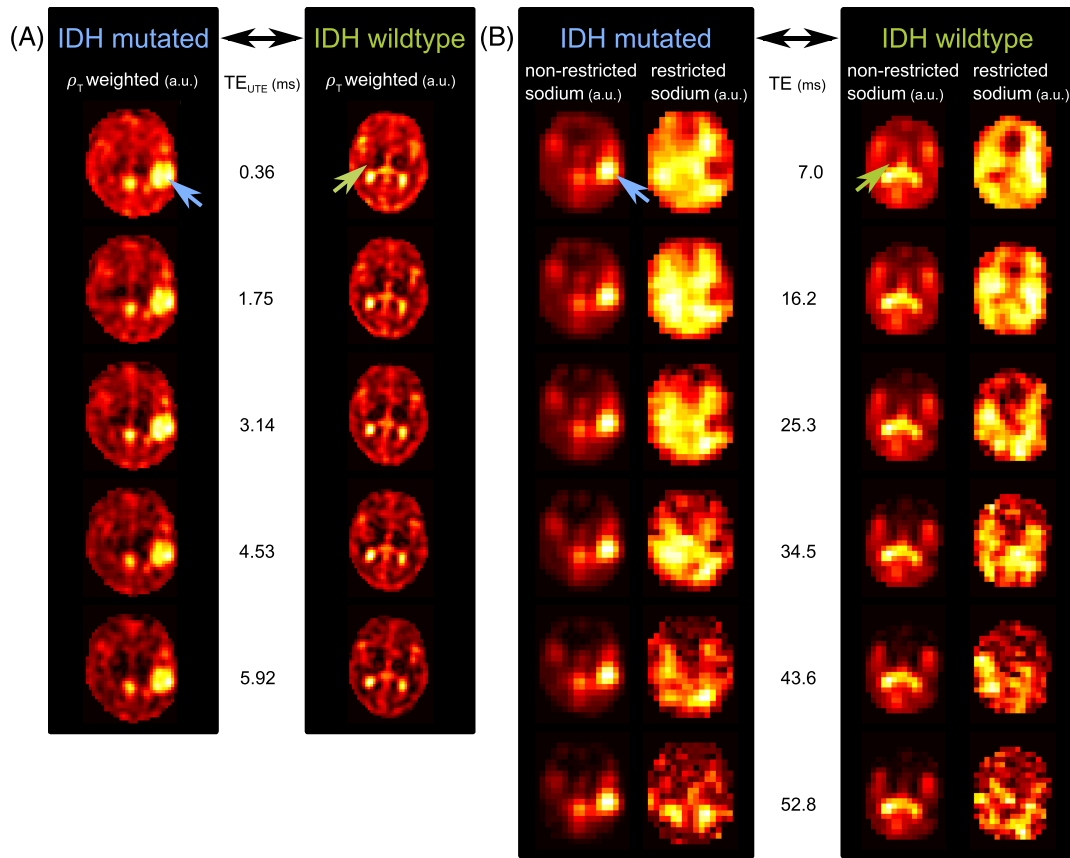


FIGURE 3 Enhanced SISTINA images of two male patients: a 38-year-old diagnosed with an IDH mutated glioblastoma WHO grade IV (blue) and a 78-year-old with an IDH wildtype anaplastic astrocytoma WHO grade III in the right basal ganglia (green). Images originate from (A) the total sodium-weighted UTE readout train and (B) nonrestricted sodium-weighted and restricted sodium-weighted gradient echoes

4.4 | Sodium relaxometry and tissue parameter quantification

From these sodium data, the following sodium parameters were estimated: the total tissue sodium concentration ρ_T , intracellular sodium concentration ρ_{in} , the ISMF χ and intracellular sodium volume fraction (ISVF) η . The methods used to calculate these parameters are given in Fleysher et al⁹ and Worthoff et al²³; of the ρ_T and ISMF the signal decay of SQ- and TQ-weighted sodium images is used, and hence ρ_{in} and ISVF can be determined for a given extracellular sodium concentration. For the quantitative estimation of the sodium concentrations the vitreous humor of the eyes was used as the reference, with a known sodium concentration of $\rho_T = 135 \text{ mmol/L}$ ^{39–41}

To estimate the relative change between tumorous tissue and healthy tissue, the following parameters were estimated from the sodium measurements: $T_{2f}^*/T_{2f,CL}^*$, $T_{2s}^*/T_{2s,CL}^*$, η/η_{CL} , χ/χ_{CL} , and $\rho_{in}/\rho_{in,CL}$, $\rho_T/\rho_{T,CL}$. This provides an instrument to evaluate the sodium tissue parameters in tumour tissue in comparison with normal-appearing CL tissue (ie, healthy tissue) within the scope of the two-compartment models (see Figure 2). Estimated relaxation times and the ratios alluded to above are given as mean and standard deviation for all patients as well as for IDH mutated and IDH wildtype groups separately. The Wilcoxon rank-sum test was used to compare sodium MRI parameters in patients with and without IDH mutation. *P*-values of .05 or less were considered significant. Statistical analyses were performed using R software.⁴²

5 | RESULTS: RELAXOMETRY AND SIMULATIONS IN NUMERICAL PHANTOMS

5.1 | UTE relaxometry: T_{2f}^* estimation method 1

The results of the simulations using T_{2f}^* estimation method 1 (Equation 1B) are presented in Figure 4A,B, Figure 5A,B, Figure A2(A,B) and Table A1. For the case observed in Worthoff et al²³ ($T_{2f}^* = 3 \text{ ms}$, $T_{2s}^* = 30 \text{ ms}$, $\chi = 0.6$, $T_{ex}^* = 55 \text{ ms}$, $\text{SNR} = 4$), the estimated fast relaxation time was $T_{2f,fit}^* = 3.62 \pm 0.72 \text{ ms}$. The relative bias Θ was 20.67% (ie, 0.62 ms), reflecting the overestimation of the value of T_{2f}^* . For other relaxation time values, Θ is shown in Figure 5A,B. At first, the simulations for SNR dependence were investigated for $\chi = 0.6$. The dependence of the fitting

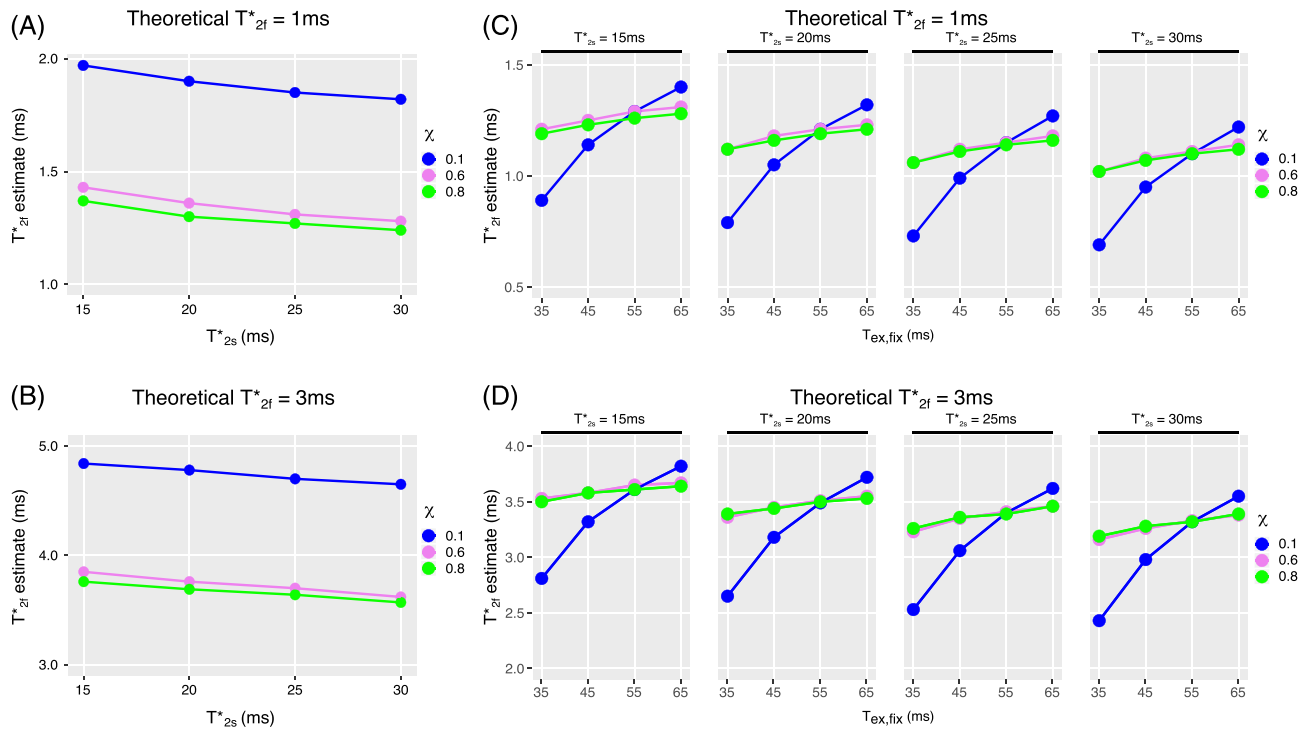


FIGURE 4 Relaxation times estimated from fitting to UTE data with method 1 (A, B) and the method 2 (C, D), simulated using a Monte Carlo method for both methods with different χ values and 16 different combinations of $T_{2s}^*/T_{ex,fix}^*$ (for method 2), for theoretical values $T_{2f} = 1$ ms (A, C) and $T_{2f} = 3$ ms (B, D)

performance of Equation 1B on the SNR of the first echo is shown in Figure A1(A,B) and the values are provided in Table A2. The minimum SNR value that delivered reliable results in the case where $T_{2f}^* = 1$ ms was SNR = 2, and in the case where $T_{2f}^* = 3$ ms, SNR = 3 (Figure A1(A,B)), which also have the lowest relative bias with a mean value of $\Theta_{\text{mean}}(T_{2f}^* = 1 \text{ ms}) = 21.38\%$ (1.21 ms) and $\Theta_{\text{mean}}(T_{2f}^* = 3 \text{ ms}) = 24.98\%$ (3.25 ms). Mean value here means that values of Θ were averaged for all considered T_{2s}^* . The higher SNR values were more reliable for the fitting routine, that is, they resulted in relative bias below a threshold deemed sufficient, in the case of the UTE data $\Theta < 30\%$. However, a saturation was observed and thus the balance between measurement time and signal dispersion can be achieved at approximately SNR = 5. At this value, Θ_{mean} remains below 25%.

Simulations for the case of $\chi = 0.1$ are provided in Table A2. The relative bias Θ varied from 57.53% to 102.65% and from 1.8 to 5.1 ms, showing a possible limitation to the reliable estimation of T_{2f}^* in tissue with low ISMF χ .

5.2 | UTE relaxometry: T_{2f}^* estimation method 2

The results of the simulations for the T_{2f}^* estimation method 2 (Equation 1C) are given in Figure 4C,D and Figure 5A,B as well as in Figure A1(C, D) and Table A3.

For the case observed in Worthoff et al.²³ ($T_{2f}^* = 3$ ms, $T_{2s}^* = 30$ ms, $\chi = 0.6$, $T_{ex}^* = 55$ ms, SNR = 4), the estimated fast relaxation time with method 2 was $T_{2f,fit}^* = 3.33 \pm 0.73$ ms. The mean value of the relative bias Θ was 11% (3.33 ± 0.73 ms), reflecting the overestimation of the value which, however, represents a 45% improvement compared with the value estimated with the T_{2f}^* estimation method 1 (Equation 1B). The performances of the methods are compared in Figure 5A,B. The highest Θ was observed for the fitting routine given by Equation 1B. In both cases, Θ decreases with increasing T_{2s}^* and increasing ISMF χ . Also for this method, the dependence of the fitting performance on the SNR values was investigated. The results are presented in and are provided in Tables A4 and A5 and Figure A1(C,D). For $\chi = 0.6$, the minimum SNR value that delivered reliable results in the case where $T_{2f}^* = 1$ ms is SNR = 2, and in the case where $T_{2f}^* = 3$ ms, SNR = 3 (Figure A1(C,D)), which also had the lowest relative bias $\Theta_{\text{mean}} = 6.60\%$ (1.07 ms) and $\Theta_{\text{mean}} = 18.17\%$ (3.55 ms) (Figure A2(C,D)).

For $\chi = 0.1$, the minimum SNR value that delivered reliable results in the case where $T_{2f}^* = 1$ ms is SNR = 9, and in the case where $T_{2f}^* = 3$ ms, SNR = 10. However, this method delivers more reliable results (lower Θ_{mean}) than the T_{2f}^* estimation method 1 for SNR > 6. Due its lower relative bias, method 2 is used to estimate the fast relaxation component T_{2f}^* .

High errors on the fitted values arose whenever the SNR was low and the nonrestricted sodium amount was high, that is, χ was low (see UTE relaxometry: T_{2f}^* estimation method 1), rendering both fitting routines for the UTE data ill-suited. Nevertheless, the fast relaxation time could be estimated from the TQ signal of the restricted sodium, as shown below.

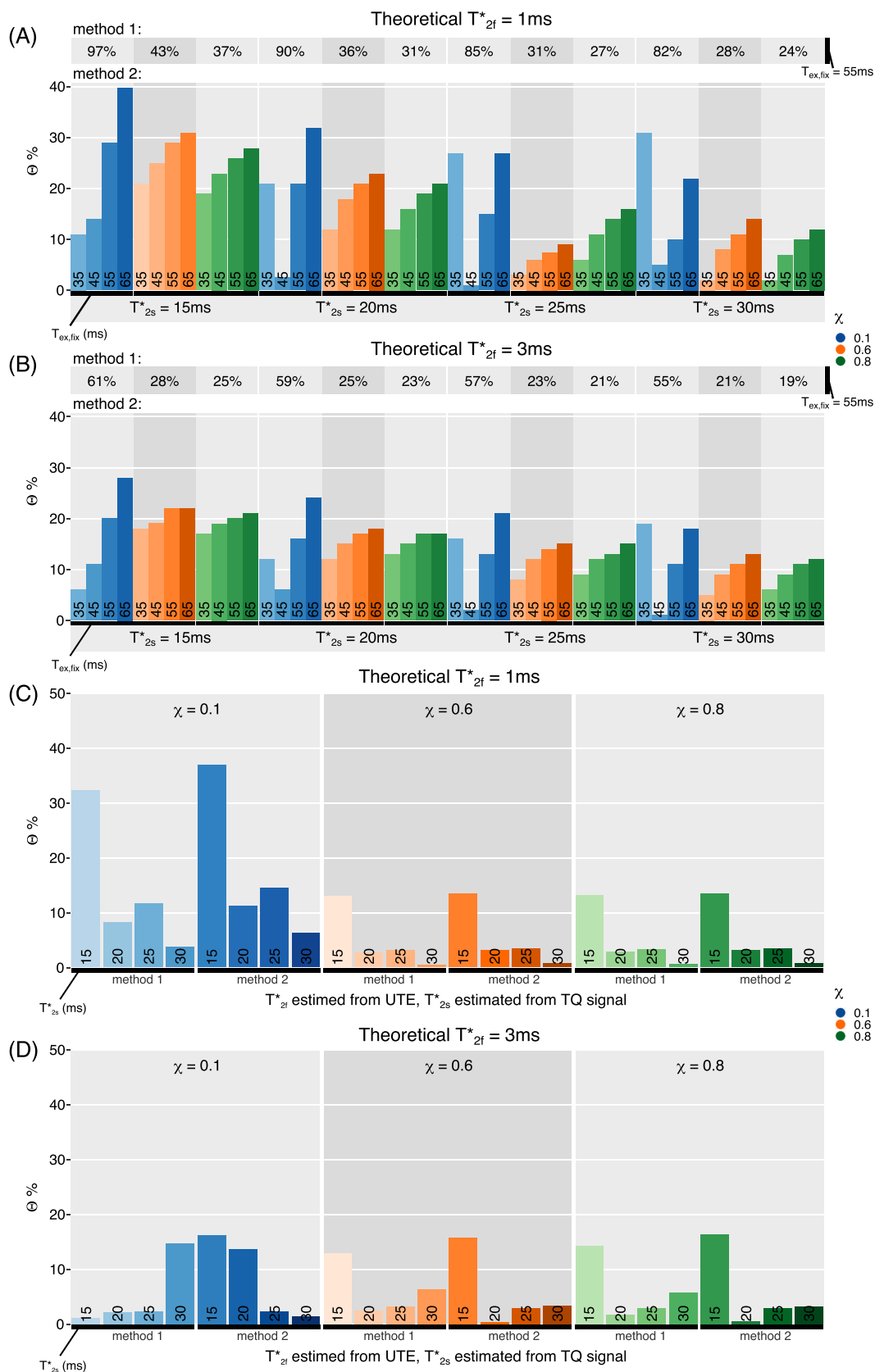


FIGURE 5 Comparison of the relative bias Θ for the UTE fitting (A, B) and for the TQ fitting (C, D) for $T_{2f}^* = 1$ ms (A, C) and $T_{2f}^* = 3$ ms (B, D) for two methods and three values of ISMF

5.3 | TQ relaxometry: T_{2s}^* estimation

The results of the fitting routine to the TQ data to estimate T_{2s}^* are given in Figure 5C,D as well as in Tables A6 (method 1) and A7 (method 2). For the case observed in Worthoff et al²³ ($T_{2f}^* = 3$ ms, $T_{2f,fit}^* = 3.62 \pm 0.72$ ms, $T_{2s}^* = 30$ ms, $\chi = 0.6$, $T_{ex}^* = 55$ ms, SNR = 6), the estimated slow relaxation time was $T_{2s,fit}^* = 28.10 \pm 0.53$ ms, and the relative bias Θ was 6.33% (1.9 ± 0.53 ms). The fast relaxation time was estimated with Equation 1C to be $T_{2f,fit}^* = 3.33 \pm 0.73$ ms, the appropriate estimated slow relaxation time was $T_{2s,fit}^* = 29.00 \pm 0.55$ ms, and the relative bias Θ was 3.33% (1 ± 0.55 ms), which was an improvement compared with method 2. Θ was low and comparable for both routines, having decreasing ISMF. The fitting routine for the estimation of T_{2f}^* given by Equation 2B, suggested in Worthoff et al,²³ is therefore reliable. However, the influence of uncertainty on the estimation of $T_{2f,fit}^*$ on the T_{2s}^* was very limited in both cases.

The dependence of the fitting routine on the SNR of the first TQC echo after the third RF pulse are shown in Figure A2(A,B) and Table A8. Due to the insignificant dependence of the routine on $T_{2f,fit}^*$, fixed values for $T_{2f}^* = 1$ ms and $T_{2f}^* = 3$ ms were assumed. The fitting routine delivered reliable results (chosen threshold for TQ data $\Theta < 20\%$) for the literature values of $T_{2f}^* = 3$ ms and $T_{2s}^* = 30$ ms for SNR larger than 3. For $T_{2f}^* = 1$ ms, the lowest limit for SNR is 4. These values give the lowest SNR limit for the reliable estimation of T_{2s}^* values.

5.4 | TQ relaxometry: combined T_{2f}^* and T_{2s}^* estimation

The TQ fit results for T_{2f}^* and T_{2s}^* estimation are given in Figure A2(C-F) and Table A9. For $T_{2f}^* = 3$ ms, the fitting results for both T_{2f}^* and T_{2s}^* had relative bias $\Theta < 8\%$ for all possible T_{2s}^* values for SNR ≥ 8 and thus are considered to be sufficient to deliver reliable fits (threshold of TQ data $\Theta < 20\%$). For the smaller SNR values, the T_{2f}^* values were underestimated, while T_{2s}^* were overestimated. However, in the literature range ($T_{2s}^* > 20$ ms⁴³), Θ is lower than the acceptable value of 20%, if SNR ≥ 5 in the case of T_{2s}^* estimation or if SNR ≥ 4 in the case of combined T_{2f}^* and T_{2s}^* estimation. Compared with the fitting routine given by Equation 1C (method 2), however, the performance of the TQ fitting of both relaxation times was better for low UTE SNR and low ISMF ($\chi = 0.1$ and SNR ($TE_{1,UTE}$) < 5). For $T_{2f}^* = 1$ ms, however, Θ of T_{2f}^* remained high.

6 | RESULTS: QUANTITATIVE PATIENT MEASUREMENTS

The combined T_{2f}^* and T_{2s}^* estimation from the TQ data (Equation 2C) was applied to tumour and CL tissue, where previously the estimation of T_{2f}^* with the UTE fitting was not possible or unreliable (SNR ($TE_{1,UTE}$) < 5). In WM with $\chi \cong 0.6$, the T_{2f}^* estimation method 2 was applied to the UTE data, delivering more reliable results in this case. The sodium tissue parameters and their ratios to healthy tissue were estimated and are given in Table 2. The statistical comparison of IDH positive and wildtype gliomas was performed. Patient #4 was not considered because of the unrealistic values of ISMF and ISVF (both > 1) due to insensitivity of the presented method in tissue with extremely low ISMF χ (as seen above). The fact that the tumour in this case possessed low χ was evident due to a high and slowly decaying UTE signal. The missing values for patient #4 and all parameters estimated for WM are provided in Tables A11-A13.

7 | DISCUSSION

7.1 | Relaxometry

The limits for the fitting routine for relaxometry are clearly evident from the simulations on the performance of the enhanced SISTINA sequence. The performance of methods 1 (Equation 1B) and 2 (Equation 1C) for estimation of T_{2f}^* from the UTE data was evaluated using Monte Carlo simulations for a number of possible combinations of theoretical values of T_{2f}^* , T_{2s}^* , T_{ex}^* , χ and SNR. Method 2 delivered reliable results for WM ($\chi = 0.6$). However, method 2 is inappropriate for a combination of low SNR and low χ .

Furthermore, the estimation of T_{2s}^* from the TQ-weighted data was evaluated with T_{2f}^* estimated using two methods. The fitting routine appeared to be mostly independent of the method used to estimate the T_{2f}^* and T_{2s}^* reliably ($\Theta < 17\%$ except for the special case: [$\chi, T_{2f}^*, T_{2s}^*, T_{ex}^*$] = [0.1, 1, 15 and 55 ms], where $\Theta \cong 32\%$).

If fitting of UTE data is unreliable due to low SNR and low χ or if the fit fails to converge, T_{2f}^* can nevertheless be estimated from TQ-weighted data instead. While the relative bias Θ for T_{2s}^* did not change significantly, the estimation of T_{2f}^* improved if SNR ($TE_{1,UTE}$) < 5 and $\chi = 0.1$. Under this condition the TQ fitting routine delivered T_{2f}^* independently of SNR ($TE_{1,CART}$).

The experiments performed here indicate that T_{2f}^* in IDH mutated tumours is shorter than in healthy CL tissue ($T_{2f}^*/T_{2f,CL}^* = 0.64 \pm 0.15$), while in IDH wildtype tumours, it was comparable ($T_{2f}^*/T_{2f,CL}^* = 0.97 \pm 0.20$). The difference in $T_{2f}^*/T_{2f,CL}^*$ between these two groups was found to be significant ($P = .05$).

TABLE 2 Results for 10 tumour patients

No.	T_{2f}^*	$T_{2f}^*/T_{2f,CL}^*$	T_{2s}^*	$T_{2s}^*/T_{2s,CL}^*$	η/η_{CL}	χ/χ_{CL}	$\rho_{in}/\rho_{in,CL}$	$\rho_T/\rho_{T,CL}$
Untreated IDH mutated gliomas								
1	0.50 ± 0.10	0.47	40.32 ± 4.81	0.97	0.77	0.42	0.99	1.79
2	1.23 ± 1.27	0.61	44.52 ± 9.20	1.30	0.60	0.13	0.52	2.34
3	2.00 ± 4.54 [#]	0.84	45.12 ± 20.62 [#]	1.45	0.64	0.29	1.06	2.28
4	---	---	---	---	---	---	---	---
5	2.43 ± 3.84 [#]	0.63	36.48 ± 16.57 [#]	1.46	0.62	0.19	0.65	2.09
Mean:	1.54 ± 0.85	0.64 ± 0.15	41.61 ± 4.03	1.30 ± 0.23	0.66 ± 0.08	0.26 ± 0.13	0.80 ± 0.26	2.12 ± 0.25
Untreated IDH wildtype gliomas								
6	2.40 ± 2.33	0.87	43.18 ± 3.63	1.67	0.79	0.55	1.10	1.59
7	2.10 ± 1.01	1.07	61.21 ± 14.05	1.86	0.80	0.55	1.48	2.24
8	3.43 ± 1.65 [#]	0.81	18.61 ± 4.03 [#]	1.21	0.89	0.70	1.22	1.52
9	5.94 ± 9.51 [#]	1.28	17.07 ± 19.54 [#]	1.12	0.99	0.89	0.91	1.01
10	4.00 ± 1.64 [#]	0.84	26.42 ± 5.83 [#]	1.32	1.02	1.26	1.30	1.06
Mean:	3.57 ± 1.53	0.97 ± 0.20	33.30 ± 18.73	1.44 ± 0.32	0.90 ± 0.11	0.79 ± 0.30	1.20 ± 0.21	1.49 ± 0.50
P-Values	.06	.05	.39	.72	.02	.02	.07	.07

[#] T_{2f}^* values were estimated with the TQ fitting routine. Additional parameters can be found in the supporting information, Tables A11-A13

However, the T_{2s}^* difference in IDH mutated and IDH wildtype tumours was found to be insignificant compared with healthy CL tissue ($T_{2s}^*/T_{2s,CL}^* = 1.30 \pm 0.23$ and $T_{2s}^*/T_{2s,CL}^* = 1.44 \pm 0.32$, respectively). Also, the difference between the two groups was found to be insignificant in T_{2s}^* ($P = .39$) and in $T_{2s}^*/T_{2s,CL}^*$ ($P = .72$).

The large fitting error on the estimated relaxation times in both tumour and normal-appearing white matter (NAWM) originate from high tumour or tissue heterogeneity and partial volume effects. In the case of very low SNR, T_{2s}^* are prone to significant error for the chosen TE (see case 7). In such a case, it is beneficial to increase the range of acquired TEs (in particular delaying the final TE appropriately) in order to improve the quality of the relaxometry data. It should be noted that parameter estimation in this study has been based on the assumption that an appropriate two-compartment model is sufficient to describe the tissue of interest, nevertheless verification of this model has not been performed.

7.2 | Quantification

The ISVF η , measured in both IDH mutated and IDH wildtype tumours, were lower than in CL tissue η_{CL} . The fraction η/η_{CL} in the IDH mutated tumours was significantly reduced compared with IDH wildtype tumours (0.66 ± 0.08 vs. 0.90 ± 0.11 with $P = .02$), meaning that the amount of extracellular sodium increased. This phenomenon could be observed if either the number of cells was reduced in the unit of volume, or if the cell volume had decreased, or both.

The ISMF χ in IDH mutated tumours was significantly lower than in CL tissue and the ratio χ/χ_{CL} was reduced compared with IDH wildtype tumours (0.26 ± 0.13 vs. 0.79 ± 0.30 with $P = .02$). The intracellular concentration ρ_{in} in IDH mutated tumours was lower than in CL tissue, in contrast to an increase in IDH wildtype tumours (0.80 ± 0.26 vs. 1.20 ± 0.21 with $P = .07$), yet these changes were statistically insignificant. A reduction might mean that the function of the sodium-potassium pump in IDH wildtype tumours was disturbed, leading to the increase in the number of sodium ions in the remaining cells.

The estimated total sodium concentration ρ_T preserved the pattern observed in Shymanskaya et al.²⁴ The fraction $\rho_T/\rho_{T,CL}$ in the IDH mutated tumours group was higher than in IDH wildtype tumours (2.12 ± 0.25 vs. 1.49 ± 0.50), and in IDH mutated tumours ρ_T was strongly increased compared with healthy tissue, yet the sample size is too small for it to be statistically significant (with $P = .07$). The increase in ρ_{in} in IDH wildtype tumours was offset by a slight decrease in intracellular volume leading to a moderate decrease in ISMF. The mechanism behind it might be cell shrinkage or a reduction of the cell number along with the disruption of the sodium-potassium pump. In IDH mutated tumours, the increase in the amount of extracellular sodium was more pronounced, however, the function of sodium-potassium pump was not disrupted, which would be evident due to the absence of an increase in ρ_{in} .

Therefore, we suggest that sodium imaging allows differentiation between IDH mutated and IDH wildtype tumours based on a possibly malfunctioning sodium-potassium pump in the latter. ISMF ratio threshold $\chi/\chi_{CL} = 0.42$ represented a sensitive parameter ($P = .02$), and allowed definite separation between both tumour types.

Here it was suggested that sodium plays an important role in tumour metabolism and that the enhanced SISTINA is sufficiently sensitive to detect these changes. While this hypothesis is supported by the statistically significant results obtained here, allowing differences in sodium metabolism between IDH mutated and IDH wildtype gliomas to be detected, several limitations of the method should be noted and addressed. The study is based on a rather small number of subjects, which limits the significance of statistical analysis. Furthermore, the resolution of the sodium-imaging sequence implemented in this study was low, which might have led to partial volume effects that could have influenced measured values, particularly when the tumorous tissue is highly heterogeneous or surrounded by edema. This disadvantage can be mitigated to some extent if ultrahigh field scanners (7, 9.4 T) are used.^{7,28} CL tissue is assumed to be healthy and unaffected by disease; great care was taken that this region did not show any visible alterations, neither in FET-PET nor proton MRI, nevertheless there is no means of verification beyond these modalities within this study.

The use of a two-compartment sodium tissue model represents a further limitation, as there is currently no consensus on sodium relaxation processes in the community. Nevertheless, the observed differences are significant, and in the scope of the assumed model, they support the theory that sodium metabolism might reflect genetic mutations.

Several studies on human brain tumours^{12,44} showed that the total sodium content in tissue could provide information on tumour response to different treatment approaches. A further study using ultrahigh field MRI has demonstrated that the ratio of intra- and extracellular sodium in cerebral gliomas can predict the IDH mutational status.⁴⁵ The findings of the present study therefore support the results observed in the literature.

8 | CONCLUSIONS

Sodium MRI using the enhanced SISTINA method is a promising tool to gauge and characterise metabolic information in brain tumours. Detailed sodium relaxometry, quantitative analysis and modelling of intra- and extracellular sodium parameters reveal abnormalities in cerebral gliomas and relate to the IDH mutational status, potentially complementing invasive biopsy and findings from PET molecular markers.

ORCID

Wieland A. Worthoff  <https://orcid.org/0000-0001-9121-8790>

Aliaksandra Shymanskaya  <https://orcid.org/0000-0001-7251-9539>

Karl-Josef Langen  <https://orcid.org/0000-0003-1101-5075>

N. Jon Shah  <https://orcid.org/0000-0002-8151-6169>

REFERENCES

1. Ostrom QT, Gittleman H, Liao P, et al. CBTRUS statistical report: primary brain and central nervous system tumors diagnosed in the United States in 2007–2011. *Neuro Oncol*. 2014;16(Suppl 4):iv1-iv63.
2. Louis DN, Perry A, Reifenberger G, et al. The 2016 World Health Organization Classification of Tumors of the Central Nervous System: a summary. *Acta Neuropathol*. 2016;131(6):803-820.
3. Langen KJ, Galldiks N, Hattingen E, Shah NJ. Advances in neuro-oncology imaging. *Nat Rev Neurol*. 2017;13(5):279-289.
4. Choi C, Ganji SK, DeBerardinis RJ, et al. 2-hydroxyglutarate detection by magnetic resonance spectroscopy in subjects with IDH-mutated gliomas. *Nat Med*. 2012;18(4):624-629.
5. Goffette SM, Duprez TP, Nassogne MC, Vincent MF, Jakobs C, Sindic CJ. L-2-Hydroxyglutaric aciduria: clinical, genetic, and brain MRI characteristics in two adult sisters. *Eur J Neurol*. 2006;13(5):499-504.
6. Sener RN. L-2 hydroxyglutaric aciduria: proton magnetic resonance spectroscopy and diffusion magnetic resonance imaging findings. *J Comput Assist Tomogr*. 2003;27(1):38-43.
7. Shah NJ, Worthoff WA, Langen KJ. Imaging of sodium in the brain: a brief review. *NMR Biomed*. 2016;29(2):162-174.
8. Madelin G, Regatte RR. Biomedical applications of sodium MRI *in vivo*. *J Magn Reson Imaging*. 2013;38(3):511-529.
9. Fleysher L, Oesingmann N, Brown R, Sodickson DK, Wiggins GC, Inglesse M. Noninvasive quantification of intracellular sodium in human brain using ultrahigh-field MRI. *NMR Biomed*. 2013;26(1):9-19.
10. Van der Maarel JRC. Thermal relaxation and coherence dynamics of spin 3/2. I. Static and fluctuating quadrupolar interactions in the multipole basis. *Concept Magn Reson A*. 2003;19a(2):97-116.
11. Madelin G, Lee JS, Regatte RR, Jerschow A. Sodium MRI: methods and applications. *Prog Nucl Magn Reson Spectrosc*. 2014;79:14-47.
12. Thulborn KR, Lu A, Atkinson IC, Damen F, Villano JL. Quantitative sodium MR imaging and sodium bioscales for the management of brain tumors. *Neuroimaging Clin N Am*. 2009;19(4):615-624.
13. Ouwerkerk R, Bleich KB, Gillen JS, Pomper MG, Bottomley PA. Tissue sodium concentration in human brain tumors as measured with ²³Na MR imaging. *Radiology*. 2003;227(2):529-537.
14. Nagel AM, Bock M, Hartmann C, et al. The potential of relaxation-weighted sodium magnetic resonance imaging as demonstrated on brain tumors. *Invest Radiol*. 2011;46(9):539-547.
15. Seshan V, Sherry AD, Bansal N. Evaluation of triple quantum-filtered ²³Na NMR spectroscopy in the *in situ* rat liver. *Magn Reson Med*. 1997;38(5):821-827.

16. Jelicks LA, Gupta RK. On the extracellular contribution to multiple quantum filtered ^{23}Na NMR of perfused rat heart. *Magn Reson Med*. 1993;29(1):130-133.
17. Dizon JM, Tauskela JS, Wise D, Burkhoff D, Cannon PJ, Katz J. Evaluation of triple-quantum-filtered ^{23}Na NMR in monitoring of intracellular Na content in the perfused rat heart: comparison of intra- and extracellular transverse relaxation and spectral amplitudes. *Magn Reson Med*. 1996;35(3):336-345.
18. Hancu I, Boada FE, Shen GX. Three-dimensional triple-quantum-filtered ^{23}Na imaging of *in vivo* human brain. *Magn Reson Med*. 1999;42(6):1146-1154.
19. Jaccard G, Wimperis S, Bodenhausen G. Multiple-quantum NMR-spectroscopy of $S=3/2$ spins in isotropic-phase - a new probe for multiexponential relaxation. *J Chem Phys*. 1986;85(11):6282-6293.
20. Keltner JR, Wong ST, Roos MS. Three-dimensional triple-quantum-filtered imaging of 0.012 and 0.024 M sodium-23 using short repetition times. *J Magn Reson B*. 1994;104(3):219-229.
21. Ridley B, Nagel AM, Bydder M, et al. Distribution of brain sodium long and short relaxation times and concentrations: a multi-echo ultra-high field ^{23}Na MRI study. *Sci Rep*. 2018;8(1):4357.
22. Woessner DE. NMR relaxation of spin-3/2 nuclei: Effects of structure, order, and dynamics in aqueous heterogeneous systems. *Concept Magnetic Res*. 2001;13(5):294-325.
23. Worthoff WA, Shymanskaya A, Shah NJ. Relaxometry and quantification in simultaneously acquired single and triple quantum filtered sodium MRI. *Magn Reson Med*. 2019;81(1):303-315.
24. Shymanskaya A, Worthoff WA, Stoffels G, et al. Comparison of [(18)F]Fluoroethyltyrosine PET and sodium MRI in cerebral gliomas: a pilot study. *Mol Imaging Biol*. 2019;22(1):198-207.
25. Garrett M, Sperry J, Braas D, et al. Metabolic characterization of isocitrate dehydrogenase (IDH) mutant and IDH wildtype gliomaspheres uncovers cell type-specific vulnerabilities. *Cancer Metab*. 2018;6(1):4.
26. Leslie TK, James AD, Zaccagna F, et al. Sodium homeostasis in the tumour microenvironment. *Biochim Biophys Acta Rev Cancer*. 2019;1872(2):188304.
27. Fiege DP, Romanzetti S, Mirkes CC, Brenner D, Shah NJ. Simultaneous single-quantum and triple-quantum-filtered MRI of ^{23}Na (SISTINA). *Magn Reson Med*. 2013;69(6):1691-1696.
28. Fiege DP, Romanzetti S, Tse DH, et al. B0 insensitive multiple-quantum resolved sodium imaging using a phase-rotation scheme. *J Magn Reson*. 2013;228:32-36.
29. Hancu I, van der Maarel JR, Boada FE. A model for the dynamics of spins 3/2 in biological media: signal loss during radiofrequency excitation in triple-quantum-filtered sodium MRI. *J Magn Reson*. 2000;147(2):179-191.
30. Gudbjartsson H, Patz S. The Rician distribution of noisy MRI data. *Magn Reson Med*. 1995;34(6):910-914.
31. Pell GS, Briellmann RS, Waites AB, Abbott DF, Lewis DP, Jackson GD. Optimized clinical T2 relaxometry with a standard CPMG sequence. *J Magn Reson Imaging*. 2006;23(2):248-252.
32. Bouhrara M, Reiter DA, Celik H, et al. Incorporation of Rician noise in the analysis of biexponential transverse relaxation in cartilage using a multiple gradient echo sequence at 3 and 7 Tesla. *Magn Reson Med*. 2015;73(1):352-366.
33. Unterrainer M, Vettermann F, Brendel M, et al. Towards standardization of 18F-FET PET imaging: do we need a consistent method of background activity assessment? *EJNMMI Res*. 2017;7(1):48.
34. Woolrich MW, Jbabdi S, Patenaude B, et al. Bayesian analysis of neuroimaging data in FSL. *Neuroimage*. 2009;45(1 Suppl):S173-S186.
35. Smith SM, Jenkinson M, Woolrich MW, et al. Advances in functional and structural MR image analysis and implementation as FSL. *Neuroimage*. 2004;23(Suppl 1):S208-S219.
36. Jenkinson M, Beckmann CF, Behrens TE, Woolrich MW, Smith SM. FSL. *Neuroimage*. 2012;62(2):782-790.
37. Sacolick LI, Wiesinger F, Hancu I, Vogell MW. B-1 mapping by Bloch-Siegert shift. *Magn Reson Med*. 2010;63(5):1315-1322.
38. Wang J, Mao W, Qiu M, Smith MB, Constable RT. Factors influencing flip angle mapping in MRI: RF pulse shape, slice-select gradients, off-resonance excitation, and B0 inhomogeneities. *Magn Reson Med*. 2006;56(2):463-468.
39. Kaufman PL, Adler FH, Levin LA, Alm A. *Adler's Physiology of the Eye*. Amsterdam, Netherlands: Elsevier Health Sciences; 2011.
40. Coe JI. Postmortem chemistries on human vitreous humor. *Am J Clin Pathol*. 1969;51(6):741-750.
41. Ouwerkerk R, Bleich KB, Gillen JS, Pomper MG, Bottomley PA. Tissue sodium concentration in human brain tumors as measured with Na-23 MR imaging. *Radiology*. 2003;227(2):529-537.
42. Team RC. *R: A language and environment for statistical computing*. Vienna, Austria: R Foundation for Statistical Computing; 2018.
43. Blunck Y, Josan S, Taqdees SW, et al. 3D-multi-echo radial imaging of ^{23}Na (3D-MERINA) for time-efficient multi-parameter tissue compartment mapping. *Magn Reson Med*. 2017;79(4):1950-1961.
44. Babsky AM, Zhang H, Hekmatyar SK, Hutchins GD, Bansal N. Monitoring chemotherapeutic response in RIF-1 tumors by single-quantum and triple-quantum-filtered ^{23}Na MRI, ^1H diffusion-weighted MRI and PET imaging. *Magn Reson Imaging*. 2007;25(7):1015-1023.
45. Biller A, Badde S, Nagel A, et al. Improved brain tumor classification by sodium MR imaging: prediction of IDH mutation status and tumor progression. *Am J Neuroradiol*. 2016;37(1):66-73.
46. Stirnberg R, Stöcker T, Shah NJ. A new and versatile gradient encoding scheme for DTI: a direct comparison with the Jones scheme. Proceedings of the 17th Annual Meeting of ISMRM, Honolulu, Hawaii, USA 2009.

SUPPORTING INFORMATION

Additional supporting information may be found online in the Supporting Information section at the end of this article.

How to cite this article: Worthoff WA, Shymanskaya A, Lindemeyer J, Langen K-J, Shah NJ. Relaxometry and quantification in sodium MRI of cerebral gliomas: A FET-PET and MRI small-scale study. *NMR in Biomedicine*. 2020;33:e4361. <https://doi.org/10.1002/nbm.4361>